NRL Report 6517

Effect of Geometry on Acoustic Monostatic Scattering from the Ocean Bottom

B.G. Hurdle and K.D. Flowers

Propagation Branch
Sound Division

March 16, 1967

U.S. Naval Research Laboratory
Washington, D.C.

Distribution of this Document is Unlimited

CONTENTS

Abstract	ii
Problem Status	ii
Authorization	ii
INTRODUCTION	1
THEORY	1
EXPERIMENTAL MEASUREMENTS	5
ANALYSIS OF MEASURED DATA	6
INTENSITY AS A FUNCTION OF TIME	6
SCATTERING STRENGTH AS A FUNCTION OF PULSE LENGTH	11
SCATTERING STRENGTH AS A FUNCTION OF GRAZING ANGLE	12
SUMMARY AND CONCLUSIONS	13
ACKNOWLEDGMENTS	13
APPENDIX A - Solution of the Normalized Incident Power	14
APPENDIX B - Effects of Refraction in Determining Scattering Strength	22
APPENDIX C - Services	25

ABSTRACT

An investigation was made to determine the degree of correspondence between measured returns scattered from the ocean bottom and an extended model of isotropic scattering from a boundary. The isotropic scattering model was applied to yield the form of the scattered intensity as a function of time for the monostatic geometry in which a circular symmetric beam function is employed. An experiment was conducted in the Blake Plateau area with a piston transducer operated at 19.5 kHz and having a beamwidth of approximately 8 degrees at the half-power points. Measured signal intensities from the relatively flat bottom in this area were averaged and compared with those of the model. These comparisons were made for depression angles between 15 and 90 degrees, and for pulse lengths between 2 and 3000 msec. Measured and computed curves were found to be essentially congruent for the range of pulse lengths and depression angles employed. However, for a given depression angle it is found that scattering strength, the acoustic constant used to characterize the boundary, varies with pulse length. This indicates that scattering from the Blake Plateau bottom is not isotropic. Measurements of scattering strength versus grazing angle for the Blake Plateau area were obtained.

PROBLEM STATUS

This is an interim report on the problem; work is continuing.

AUTHORIZATION

NRL Problem S01-12
Projects RF 101-03-44-4059 and SF 101-03-15-8181

Manuscript submitted November 28, 1966.

EFFECT OF GEOMETRY ON ACOUSTIC MONOSTATIC SCATTERING FROM THE OCEAN BOTTOM

INTRODUCTION

When an area of the ocean bottom is ensonified, a portion of the energy penetrates into and is lost in the bottom, and the remainder is returned to the water. If the directivity function of the original source is preserved in that portion returned to the water, the process can be considered as that of reflection. If on the other hand the directivity function of the energy returned from the bottom is distorted, the process can be considered as one of scattering. The degree of scattering can change from that causing small distortions to that causing radical distortions of the original directivity function.

This report is concerned with the scattering of sound from the bottom back to the source point (the monostatic case, i.e., source and receiver point coincident) when a directive source is employed. The purpose of this report is to determine the degree of correspondence between the scattering indicated by isotropic scattering theory and that measured in a monostatic scattering experiment.

THEORY

The analysis of this paper is based on the isotropic scattering model by Eckart* except following Urick† scattering strength is used rather than the scattering coefficient. The model states that

$$I_s = s I_i A \tag{1}$$

where I_s is the intensity of the scattered signal at unit distance (1 yard) from the boundary, s is the scattering strength, I_i is the incident intensity, and A is the ensonified area contributing to the scattered signal at a particular instant.

A practical acoustical experiment employing transducers having a beam function requires the integration of the incident intensity over the ensonified area. Using Cartesian coordinates the scattered intensity is

$$I_s(\Psi) = \iint_A s(x, y)\ I_i(x, y)\ dxdy \tag{2}$$

where $s(x,y)$ is the scattering strength of $dxdy$ in the direction Ψ.

In extending the isotropic model to accommodate a directive source, it is convenient to use polar coordinates. Equation (2) is rewritten as

$$I_s(\Psi) = \iint_R s(\delta,\theta)\ I_i(r,\delta,\theta)\ dR \tag{3}$$

*Carl Eckart, "Principles and Applications of Underwater Sound," NDRC Summary Technical Reports, Division 6, Vol. 7, Washington, D.C., 1946.

†R.J. Urick, "The Backscattering of Sound from a Harbor Bottom," J. Acoust. Soc. Am. 26:231 (1954).

where I_s is the scattered intensity at unit distance (1 yard) in the direction Ψ as shown in Fig. 1, where Ψ is the angle of scatter observation, R is the region of ensonification, s is the scattering strength, r is the distance between the source and dR, δ is the angle between the direction of incident intensity and the horizontal or grazing angle, and I_i is the incident intensity on dR.

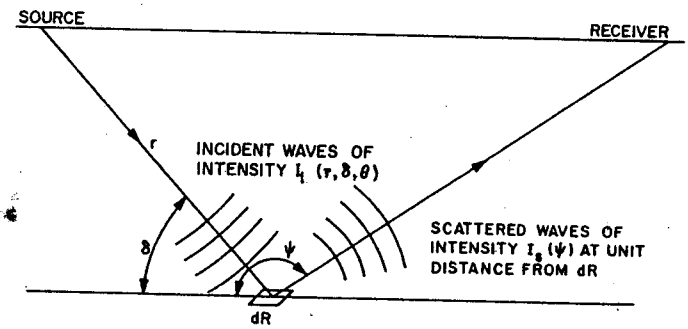

Fig. 1 - General scattering geometry

For the monostatic case we let $\Psi = \beta$, where

$$\beta = \frac{\delta_{max} + \delta_{min}}{2} \tag{4}$$

is the angle of the center ray of the source-receiver beam function with respect to the horizontal (Figs. 1 and 2). We also restrict the model to a beam function with circular symmetry about the beam axis.

Although the scattering strength is dependent on the geometry, particularly on β, if $|s(\delta) - s(\beta)|$ for $\delta_{min} \leq \delta \leq \delta_{max}$ is sufficiently small, a constant $s(\beta)$ over the interval may be used. This allows s to be removed from the integral but restricts the model to small beamwidths. Including the above restrictions in Eq. (3) results in

$$I_s(\beta) = s(\beta) \int_R \int I_i(r, \delta, \theta)\, dR \tag{5}$$

where the geometry is illustrated in Fig. 2. Then

$$NP_i = \int_R \int I_i(r, \delta, \theta)\, dR \tag{6}$$

where P_i is the normalized incident power and N is a constant.

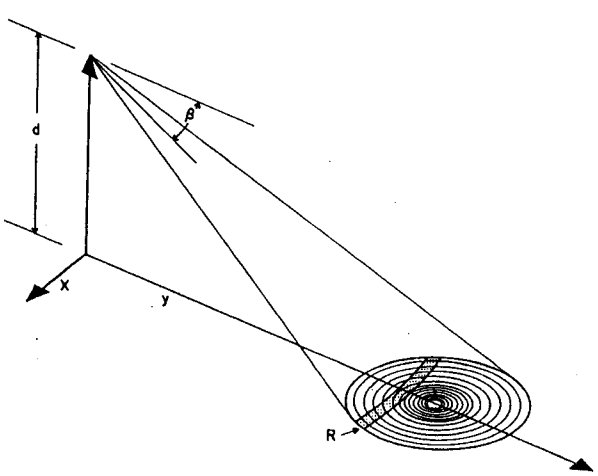

Fig. 2 - Geometry for monostatic scattering with a directive source

Since the incident power on the bottom boundary is the integral of the incident intensity over the ensonified area, it is independent of distance, except for attenuation; i.e., there is no power loss in transit from the source to the bottom except for attenuation losses. This enables P_i to be evaluated at unit distance from the source-receiver.

In taking account of the beam function, which is directly proportional to $I_i(r, \delta, \theta)$, it is found that most functions are sufficiently complicated to make the necessary integration intractable. Further, when making a computation on a particular transducer that is to be employed in obtaining experimental data, it is considered better to use the measured function of the transducer, which is never exactly analytic. For these reasons the measured beam function was used and incremented to enable a numerical integration of P_i.

Since the same directivity function is used in transmission and reception, it is convenient to use the square of the function rather than deal with it independently in both transmission and reception. Therefore, the square of the directivity function is illustrated in Fig. 3.

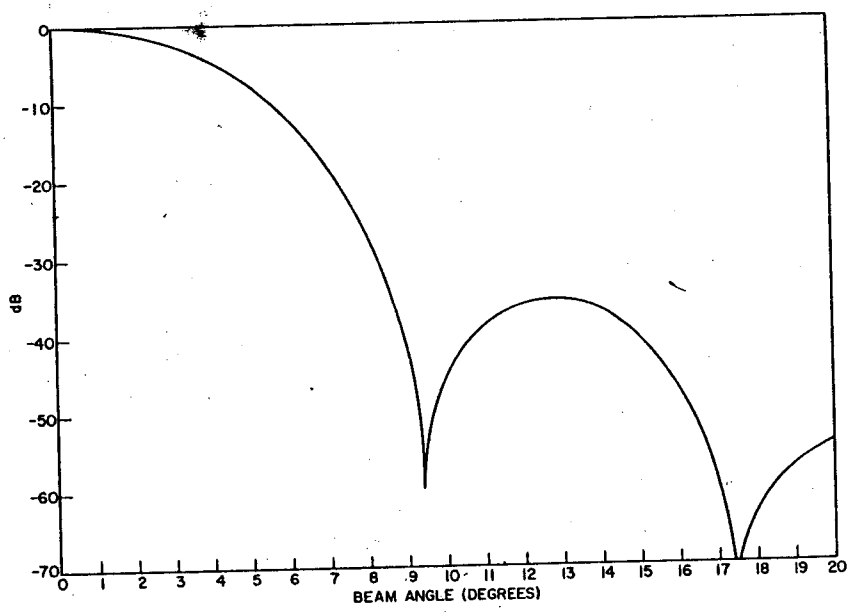

Fig. 3 - Square of the source-receiver beam function at 19.5 kHz

By introducing the propagational velocity a transformation of the variable is made so that the incident power can be evaluated as a function of time for the parameters pulse length and grazing angle. The details of the P_i solution are contained in Appendix A.

A computer program was constructed to make the evaluation. Several curves of P_i versus time for a variation of pulse length and a constant grazing angle are illustrated in Fig. 4. A similar set illustrated in Fig. 5 gives P_i as a function of time for a constant pulse length and several grazing angles. All of the curves are for a constant-amplitude transmitted pulse of length τ.

The steady state value of P_i of -19.1 dB indicated by the flat portion of the 500-msec curve in Fig. 5 is in agreement with the value computed for the transducer using the Christensen* method.

*R.J. Christensen, et al., "The Discrimination of Transducers Against Reverberations," OSRO 6.1-SR30-968, Aug. 31, 1943.

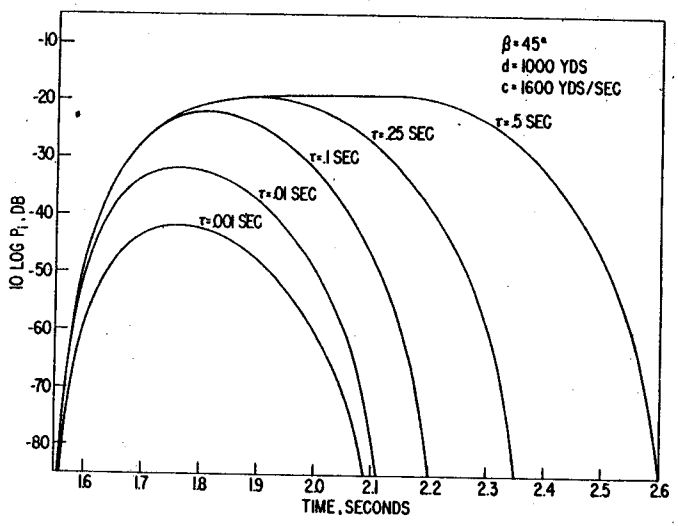

Fig. 4 - Normalized incident power as a function of time for various pulse lengths with the depression angle constant

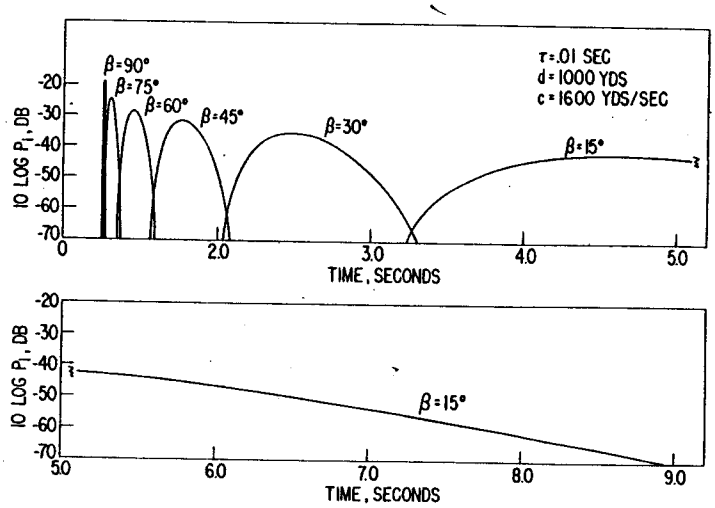

Fig. 5 - Normalized incident power as a function of time for various depression angles with the pulse length constant

The discussion to this point has been concerned with quantities in the vicinity of the scattering boundary. In practice, both the source and receiver are a distance r from the boundary. This requires that the propagation to and from the boundary plus the transducer characteristics be included. Thus for the incident path (using the dB form)

$$10 \log NP_i = L + 20 \log i - D - Kr + 10 \log P_i \tag{7}$$

where L is the transmitting response (dB//1 μbar at 1 yd/ampere), i is the source current (amperes), D is the dome loss (dB), and K is the absorption coefficient (dB/yd).

Taking account of the receiving characteristics,

$$10 \log I_s = E - M - G + 20 \log r + Kr + D \tag{8}$$

where E = 20 log (amplitude of received signal) (dB//1 volt), M is the receiving sensitivity (dB//1 volt/μbar), G is the receiving gain (dB), K is the absorption coefficient (dB/yd), and D is the dome loss (dB). Then

$$S = (E - M - G + 20 \log r + Kr + D) - (L + 20 \log i - D - Kr + 10 \log P_i) \tag{9}$$

where $S = 10 \log s$. For an isotropic medium Eq. (9) is written in terms of depth d and depression angle β using the relation $r \sin \beta = d$:

$$S = E - M - G - L - 20 \log i + 2D + 20 \log d + 20 \log (csc\, \beta) + 2Kd(csc\, \beta) - 10 \log P_i. \tag{10}$$

EXPERIMENTAL MEASUREMENTS

In order to compare the predicted envelope of the scattered signals with those of measured returns from the ocean bottom an experiment was conducted in the Blake Plateau. The area in which the measurements were made is illustrated by the rectangle in Fig. 6. This area was chosen because of the relative flatness of the bottom, where the water depth varied less than ±1 fathom over the area where measurements were taken, and because of the uniformity of the bottom material, which consisted of a calcareous sediment, as indicated by corings.

The instrumentation consisted of a special sonar operating at 19.5 kHz. The special features of the sonar included a piston transducer mounted in the bow of a submarine that could be directed throughout the forward hemisphere. Its beamwidth is approximately 8 degrees to the half-power points with all side lobes being down 17 dB or more. Figure 3 illustrates the square of the beam function between the axis and the second side lobe. The time duration of transmitted pulses was controlled by a counter in 1-msec increments, enabling the pulse length to be varied from 2 msec to 3000 msec. The instrumentation also provided for recording the bottom scattered returns, with time base and amplitude calibration. Details of the instrumentation system employed are contained in NRL Memorandum Report 1767.*

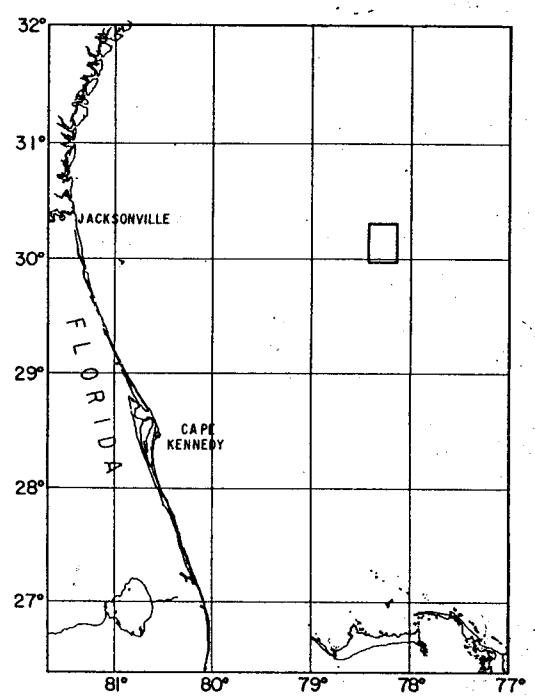

Fig. 6 - Operating area

A series of runs were made for a series of depression angles, pulse lengths, and speeds. All parameters were held constant for a particular run, while recordings of the monostatic scattered signal were made

*H.U. Criss, K.D. Flowers, B.G. Hurdle, R.M. Lee, and K.P. Thompson, "Procedures for a Series of Experiments in Acoustic Scattering from the Ocean Bottom and Volume in the Blake Plateau Area," NRL Memorandum Report 1767, April 17, 1967.

for 20 to 100 returns. Environmental data was taken periodically during the experiment to enable the computation of refractive effects of the medium in this area. These computations included the sound speed profile, the average sound speed over the path as a function of the depression angle, the angle of arrival at the bottom as a function of the depression angle at the surface, the spreading loss over the path as a function of angle, and other pertinent characteristics of the propagation (see Appendix B).

ANALYSIS OF MEASURED DATA

The amplitude envelope was recorded in analog form (on a dB scale) as a function of time for each return. The data was then incremented in 10 to 25 msec steps throughout the duration of the return and converted to digital form with the aid of a data reader. Care was taken to retain the time of each reading from t_0 the leading edge of the transmitted pulse. The power ratio of each value e_i^2 was averaged over the number of returns recorded for each time increment throughout the return, i.e.,

$$E_i = 10 \log e_i^2$$

and

$$\langle e^2 \rangle = \frac{1}{n} \sum_{i=1}^{n} e_i^2 \Big|_{t=c} \tag{11}$$

where n is the number of returns and c is a constant. The mean value of the envelope was then converted to dB by

$$\langle E \rangle = 10 \log \langle e^2 \rangle . \tag{12}$$

This makes $\langle E \rangle \propto \langle I \rangle$ assuming that the intensity is proportional to pressure squared.

The light line of Fig. 7 illustrates the envelope of a single return as a function of time. The form of the signal envelope, including the large-amplitude fluctuations, is consistent with previous fluctuation studies.* The heavy line illustrates the mean envelope $\langle E \rangle$. Only the first bottom return with a few points from the decaying volume reverberations and part of a second bottom return are included in the average envelope illustrated. Some of the variations in level of the mean envelope at the beginning of the return are caused by variation in the amplitude of the transmitted pulse in that region, caused by the power supply response of the driver amplifier. The shaded area about the mean envelope is the 95-percent-confidence interval.† The interval is approximately ±1 dB about the mean.

INTENSITY AS A FUNCTION OF TIME

Figures 8 through 13 compare the shape of the envelope predicted by the model (solid curve) and the mean intensity from measured data (points). The solid curves were obtained from the solution of Eq. (6) with the appropriate parameters of pulse length and grazing angle. The points were obtained as described above using Eqs. (8) and (12). The scale along the abscissa is time in seconds of the return sequence.

---

*B.G. Hurdle, R.H. Ferris, and K.D. Flowers, "Effect of Transducer Velocity on the Structure of Signals Scattered from the Ocean Bottom," J. Acoust. Soc. Am. 36:1931 (1964).

†C.C. Peters and W.R. Van Voorhis, "Statistical Procedures and Their Mathematical Bases," New York: McGraw-Hill, 1940.

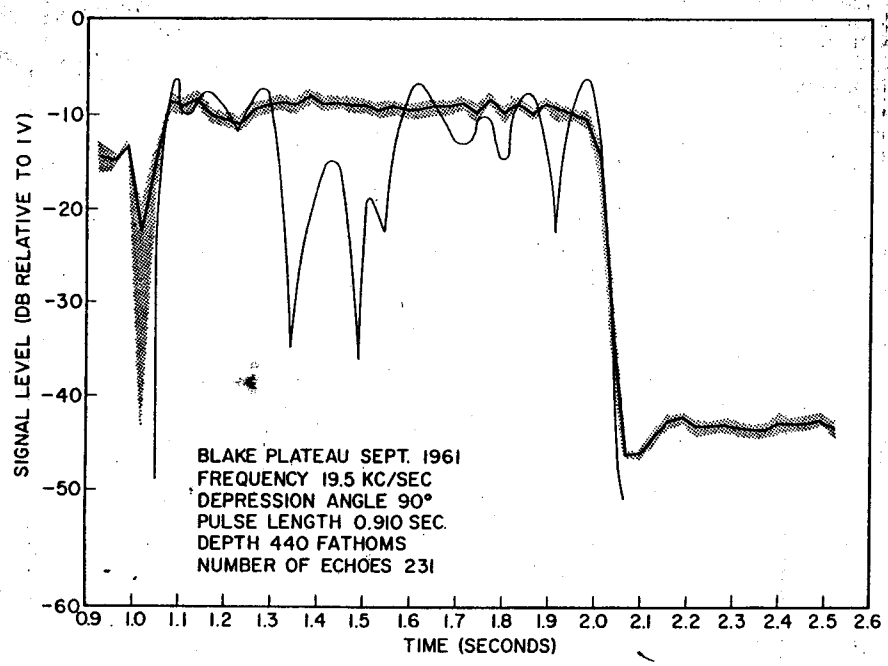

Fig. 7 - Envelope of a single return and the mean envelope of the bottom scattered signal as a function of time

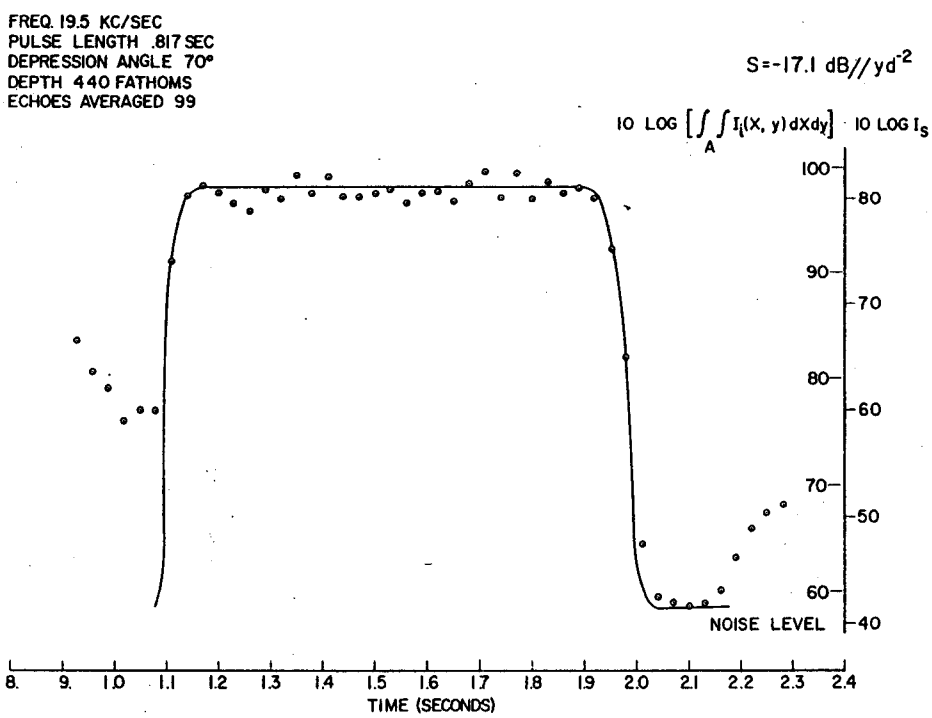

Fig. 8 - Measured bottom scattered signals and the predicted envelope as a function of time

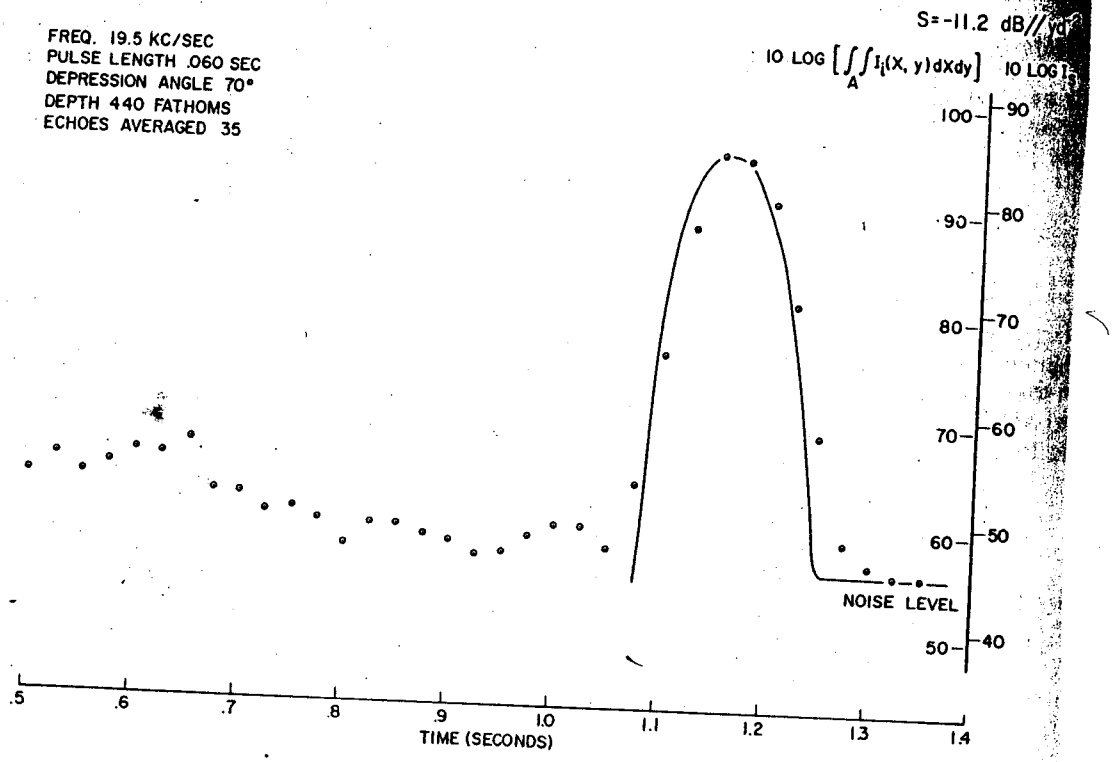

Fig. 9 - Measured bottom scattered signals and the predicted envelope as a function of time

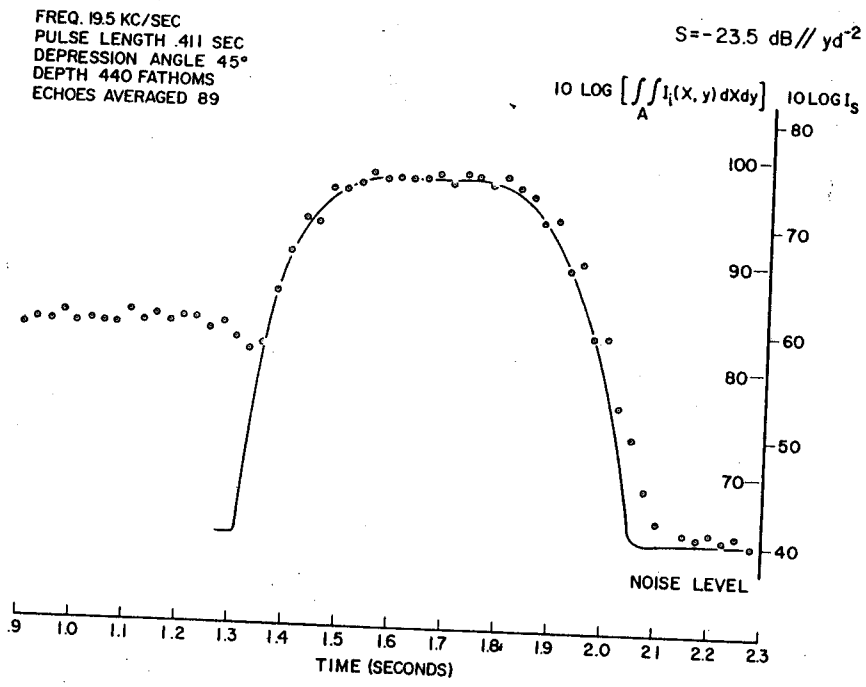

Fig. 10 - Measured bottom scattered signals and the predicted envelope as a function of time .

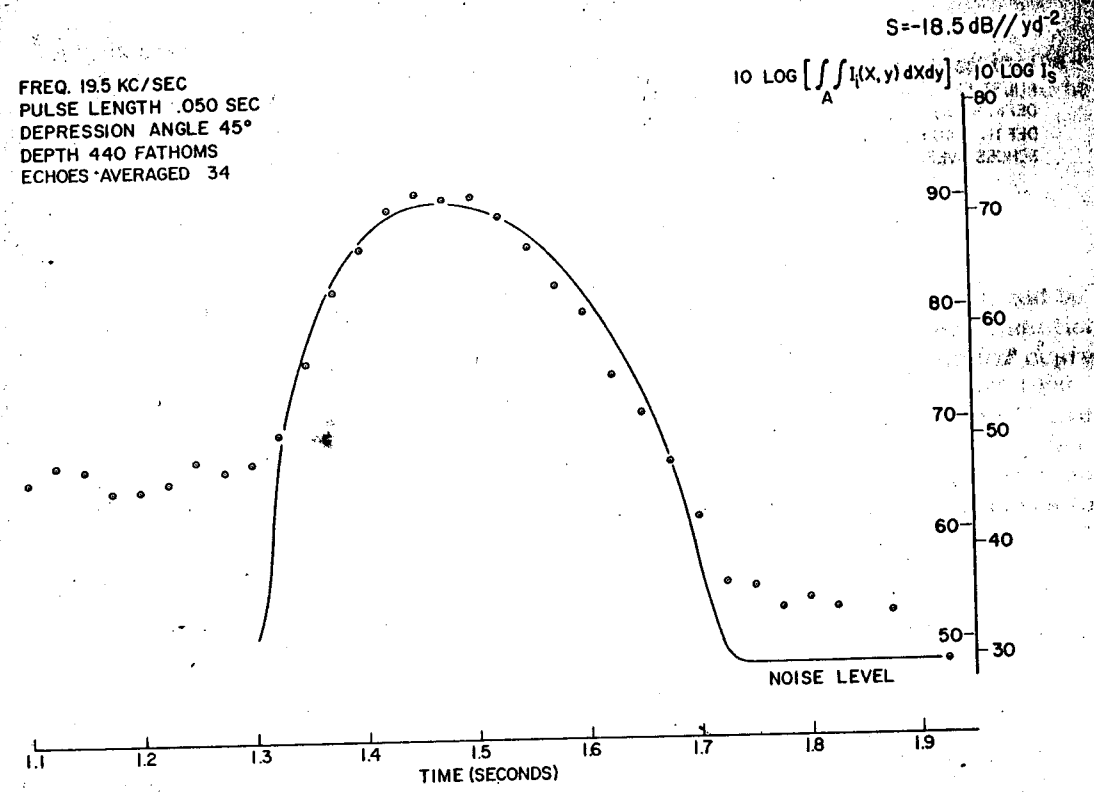

Fig. 11 - Measured bottom scattered signals and the predicted envelope as a function of time

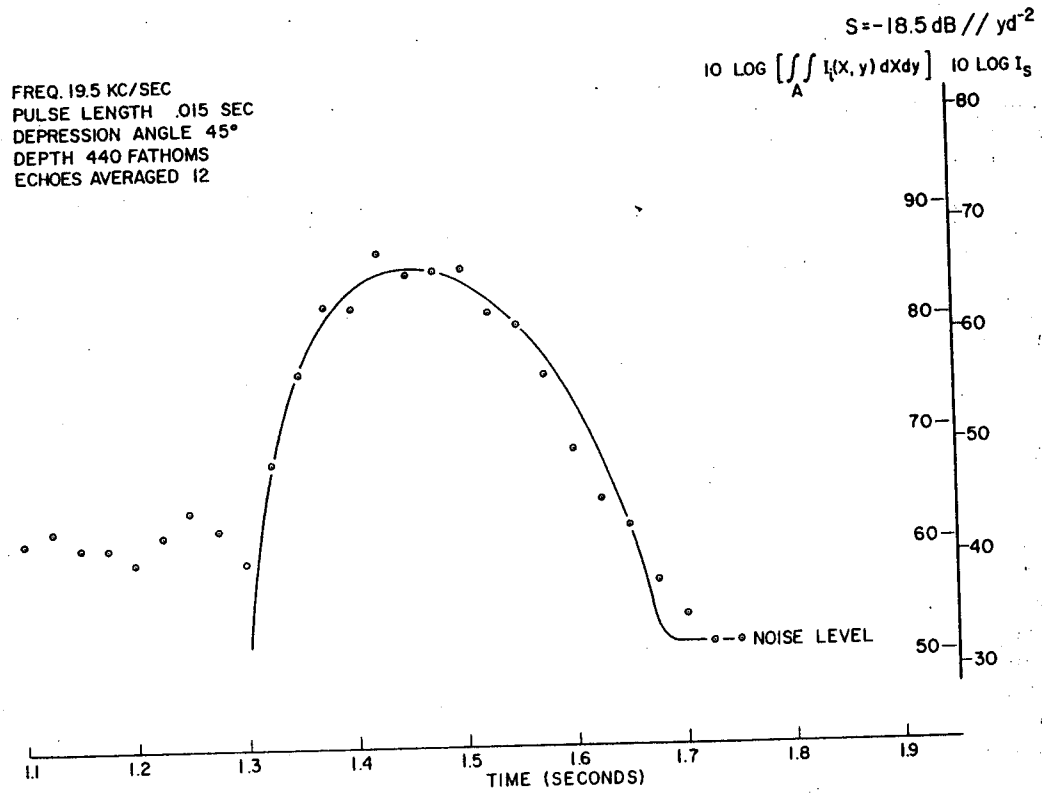

Fig. 12 - Measured bottom scattered signals and the predicted envelope as a function of time

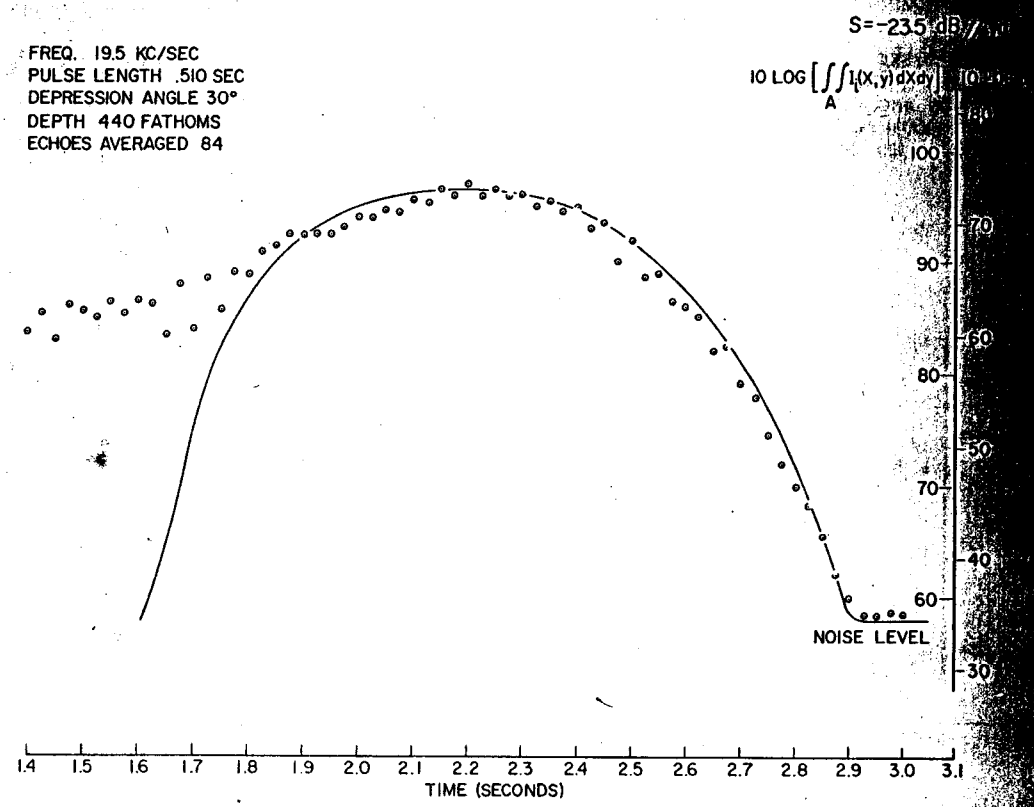

Fig. 13 - Measured bottom scattered signals and the predicted envelope as a function of time

Some of the volume reverberations can be seen prior to the initiation of the bottom return, particularly at the longer pulse lengths. For the shorter pulse lengths, exemplified in Fig. 9, the reverberations have decayed to or near the noise level prior to the initiation of the bottom return. For the longer pulse lengths, exemplified by Figs. 8 and 10, a steady state condition is reached (at approximately 1.15 seconds in Fig. 8) when the pulse length is sufficiently long to provide a simultaneous contribution from all of the area defined by the beam. At approximately 1.9 seconds in the same figure the return starts to decay as the pulse moves off the area. The noise level is noted at the end of the bottom return and part of a second bottom return is seen between 2.15 and 2.3 seconds. During the steady state portion of the return the spread of the points about the curve is approximately ±1.5 dB.

The two scales on the right side of Figs. 8 through 13 correspond to the curve and the points respectively. The scale on the left side of the line represents power incident on the bottom, and the one on the right side represents the intensity of the scattered signal 1 yard from the bottom. The curves have been positioned vertically until the best fit was reached. The distance moved (dB) in fitting the curves corresponds to the scattering strength. The numerical value of scattering strength is obtained by reading the difference between the two dB scales. For example, the scattering strength for the data in Fig. 8 is -17.1 dB//yd^{-2}. Note the degree of fit between the measured and predicted envelopes in Fig. 9, for a depression angle of 70 degrees and a pulse length of 60 msec, the major feature is that the pulse length is less than that required for steady state. Note the 2-to-1 expansion of the time scale in this figure as compared with Fig. 8.

Figures 8 through 13 are six sets from among approximately 70 sets of data analyzed and represent the envelope forms experienced and type of agreement obtained between predicted and measured envelope forms of the scattered signals.

SCATTERING STRENGTH AS A FUNCTION OF PULSE LENGTH

If the scattering from the boundary is isotropic, the scattering strength should be independent of pulse length or the dimensions of the insonified area, all other conditions remaining constant. To test this hypothesis a series of data sets were taken for depression angles of 45 and 70 degrees with pulse lengths varying between 2 msec and 1000 msec. Scattering strengths were computed as indicated above. Figures 14 and 15 are illustrations of scattering strength as a function of pulse length for depression angles of 45 and 70 degrees, respectively. Figure 14 shows that the scattering strength increases as pulse length increases, to a maximum at approximately 75 msec, then decreases to

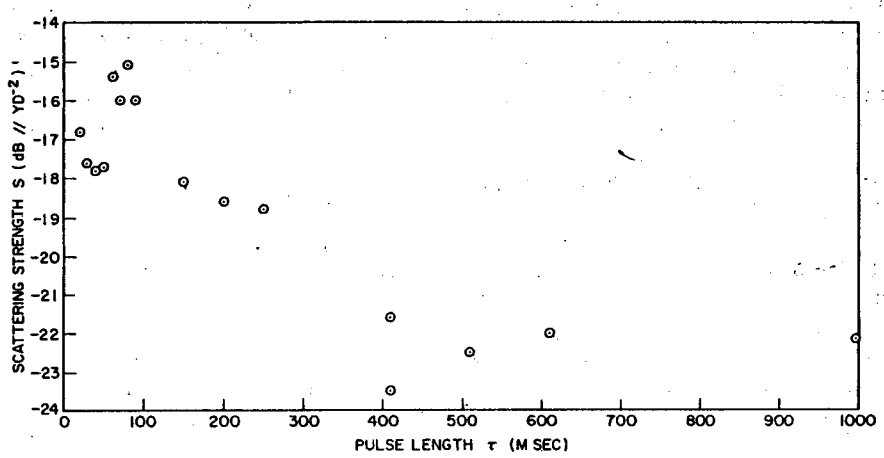

Fig. 14 - Scattering strength as a function of pulse length at a depression angle of -45 degrees

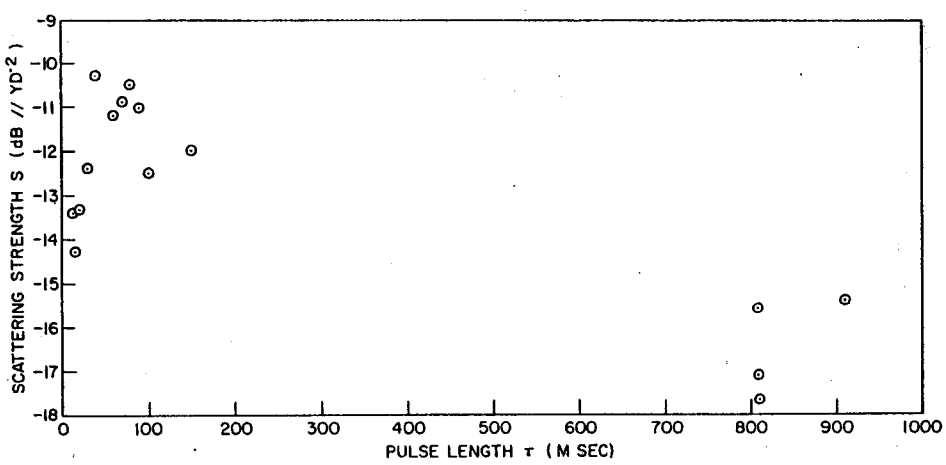

Fig. 15 - Scattering strength as a function of pulse length at a depression angle of -70 degrees

become constant, within experimental error, when it is sufficiently long to provide a steady state portion in the return at about 400 msec or greater. Although the data for 70 degrees in Fig. 15 are not as complete, the same trend is observed.

These data indicate that the scattering strength is not constant with pulse length except in the steady state region. Here it is constant within the ±1-dB experimental spread. Further, since the area and configuration of the contributing area are constant for all pulse lengths in the steady state region, the effect is probably not a function of the pulse length but of the contributing area or the dimensions making up the configuration of the area. The major change of this configuration is in the dimension of the pulse along the major axis of the ellipse, where the dimension becomes small relative to the length of the major axis for the shorter pulse lengths.

The variation of scattering strength with pulse length would seem to be reflected in the fit of the leading and trailing edges in the envelopes of Figs. 8 through 13. It should be remembered that during the rise and decay of the envelope the effective scattering area is continuously changing in magnitude, which is equivalent to a continuously changing pulse length. Experimentally the difficulty of precisely defining the leading and trailing edges of the return and the averaging process obscures any change of scattering strength that might be present. This means that the constancy of scattering strength as a function of pulse length is a more sensitive indicator of isotropy than the degree of fit of the experimental and predicted envelopes.

SCATTERING STRENGTH AS A FUNCTION OF GRAZING ANGLE

Data for the monostatic scattering strength versus grazing angle are illustrated in Fig. 16. The abscissa is in terms of the grazing angle at the bottom. The curve is faired through the measured points. Each point represents a value obtained in the same manner as discussed previously. The data is for the steady state condition, pulse lengths varying from 410 to 3050 msec. Runs were made in various directions over the bottom in the operating area (Fig. 6) and analyzed for variations in scatter strength with geographical orientation. No dependence of orientation could be detected in the scattering strength.

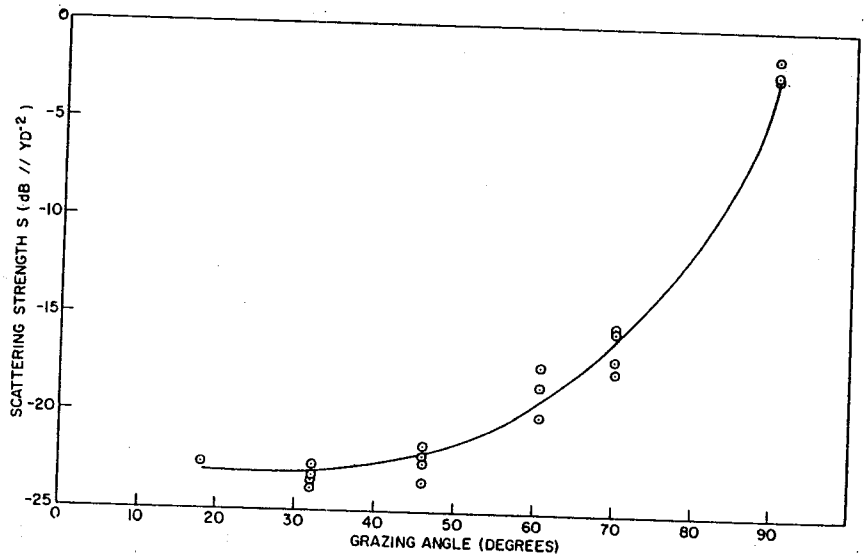

Fig. 16 - Scattering strength as a function of grazing angle

Refraction of the medium has been taken into account in the manner described in Appendix B.

SUMMARY AND CONCLUSIONS

The model for isotropic scattering from a boundary has been extended to accommodate a conical acoustic geometry for the monostatic case. The model has been evaluated and compared with measured data with reasonable agreement.

However, significant variation of scattering strength with pulse length indicates that the bottom investigated is not truly an isotropic scatterer. Additional work is planned to provide further information on this effect. The variation of scattering strength with pulse length or the characteristic dimensions of the scattering area raises a serious question as to the comparability of the measured scattering data when all of the parameters are not identical. Thus there is increased urgency to provide a model explaining this variation in order that a scattering strength or other appropriate constant can be obtained that is independent of everything except the characteristics of the boundary.

ACKNOWLEDGMENTS

The authors acknowledge with sincere thanks and appreciation the following people whose efforts have made this work possible: John P. Campbell, A. L. Gotthardt, Harry U. Criss, Robert M. Lee, and Dennis L. Wilson.

The authors are particularly grateful for the excellent cooperation of the officers and crew of USS Grouper (AGSS-214). Specific services rendered are contained in Appendix C.

Appendix A

SOLUTION OF THE NORMALIZED INCIDENT POWER

Starting with Eq. (6) of the text

$$NP_i = \int_R\int I_i(r, \delta, \theta)\, dR \tag{A.1}$$

P_i, the normalized incident power on the bottom boundary, is the integral of the incident intensity over the ensonified area. Thus, P_i is independent of distance, except for attenuation, and of orientation of the ensonified area; i.e., there is no power loss in transition to the bottom except for attenuation losses. The method used then will be to evaluate P_i at unit distance from the source-receiver.

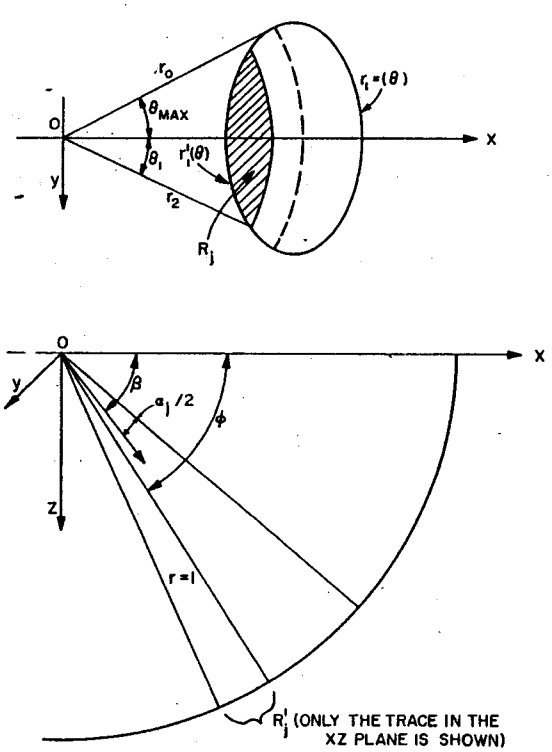

Fig. A1 - Geometry for calculating the normalized incident power at unit distance

Referring to Fig. A1, the surface region R_j' is that portion of the sphere of unit radius contained between the cone of vertex angle α_j and the cone of vertex angle $2(90 - \phi)$. When R_j' is projected on the xy plane, we get the region R_j. The area of R_j' is

$$A_j = \int_{R_j'}\int dR_j' = \int_{R_j}\int \sec\gamma\, dR_j \tag{A.2}$$

where γ is the angle between the tangent plane of a surface element on the spherical cap and the xy plane. The spherical cap is that portion of the surface of the sphere of unit radius contained within the cone of vertex angle α_j.

The beam function, which is directly proportional to $I_i(r, \delta, \theta)$, is a characteristic of the source-receiver. Most beam functions are sufficiently complicated to make the necessary integrations intractable. Thus, we increment the beam function to enable the numerical integration of P_i. This means that we have a finite sum of area-intensity products, as illustrated in Fig. A2.

If

R_n = total ensonified area,

R_j = total ensonified area contained in the jth ellipse,

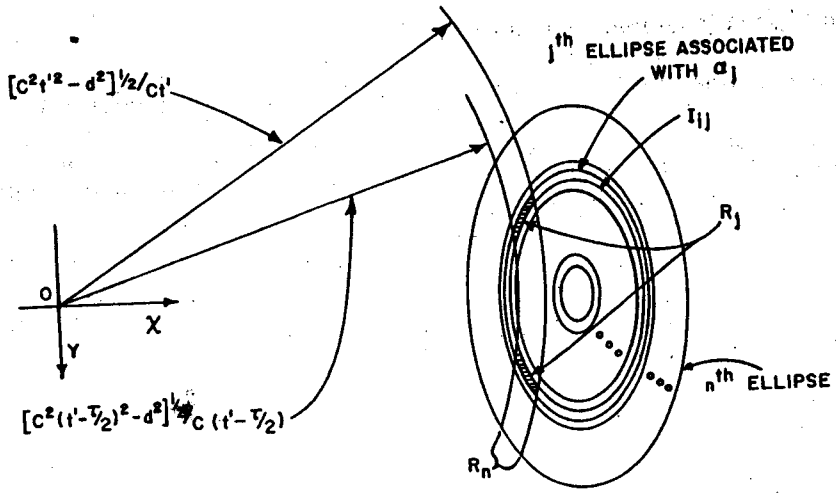

Fig. A2 - Geometry of the finite sum of area-intensity products

$A_j(t')$ = that area bounded by the jth ellipse and the circle of radius $[c^2t'^2 - d^2]^{1/2}/ct'$, and

$A_j(t' - \tau/2)$ = that area bounded by the jth ellipse and the circle of radius

$$\frac{\left[c^2\left(t' - \frac{\tau}{2}\right)^2 - d^2\right]^{1/2}}{c\left(t' - \frac{\tau}{2}\right)},$$

then

$$P_i(t') = \int_{R_n}\int I_i(r, \delta, \theta)\, dR_n \approx \sum_{j=1}^{n} I_{ij}(R_j - R_{j-1}) \tag{A3}$$

$$= \sum_{j=1}^{n} I_{ij} \left\{\left[A_j(t') - A_j\left(t' - \frac{\tau}{2}\right)\right] - \left[A_{j-1}(t') - A_{j-1}\left(t' - \frac{\tau}{2}\right)\right]\right\} \tag{A4}$$

or

$$P_i(t) = \sum_{j=1}^{n} I_{ij} \left\{\left[A_j\left(\frac{t}{2}\right) - A_j\left(\frac{t}{2} - \frac{\tau}{2}\right)\right] - \left[A_{j-1}\left(\frac{t}{2}\right) - A_{j-1}\left(\frac{t}{2} - \frac{\tau}{2}\right)\right]\right\}, \tag{A5}$$

where prior to the arrival of the wave on the boundary

$$A_0(t') = A_0\left(t' - \frac{\tau}{2}\right) = 0,$$

$t' = d/c \sin\phi$ = transit time to the bottom via the path associated with ϕ,

τ = pulse duration,

d = water depth,

c = sound speed (assumed constant), and

$t = 2t'$ is the time $P_i(t')$ is contributing to the signal received at the source point.

It remains to express $A_j(t)$ explicitly. This is done by letting $u = t/2$ or $u = (t-\tau)/c$ and determining $A_j(u)$. It is convenient to consider three separate cases as determined by the tilt angle β and/or the angle α_j:

Case 1: $\beta = \pi/2$ (Fig. A3)

$$A_j(u) = 0, \qquad u \le u_0 \tag{A6}$$

$$A_j(u) = 2\pi[1 - (d/cu)], \qquad u_0 < u < u_2 \tag{A7}$$

$$A_j(u) = 2\pi[1 - \cos(\alpha_j/2)], \qquad u_2 \le u; \tag{A8}$$

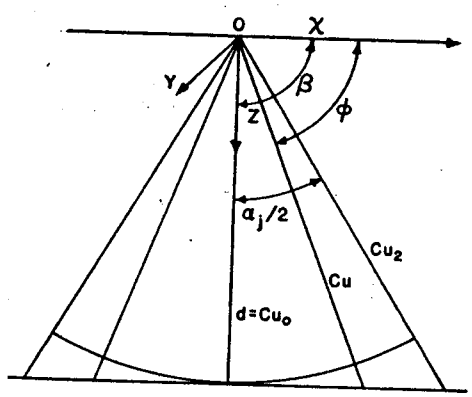

Fig. A3 - Geometry for case 1

Case 2: $\beta + (\alpha_j/2) \le \pi/2$ (Fig. A4)

$$A_j(u) = 0, \qquad u \le u_1 \tag{A9}$$

$$A_j(u) = \pi[1 - \cos(\alpha_j/2)] - \frac{2\theta_1 d}{cu} + 2\cos(\alpha_j/2)\cos^{-1}\left[\frac{\cos\theta_1}{(1-\cos^2\beta\sin^2\theta_1)^{1/2}}\right]$$
$$\pm 2\left\{\cos^{-1}\left[\cos\beta\csc(\alpha_j/2)\sin\theta_1\right] - \cos(\alpha_j/2)\cos^{-1}\left[\frac{\cot(\alpha_j/2)\cos\beta\sin\theta_1}{(1-\cos^2\beta\sin^2\theta_1)^{1/2}}\right]\right\},$$
$$u_1 < u < u_2, \tag{A10}$$

$$A_j(u) = 2\pi[1 - \cos(\alpha_j/2)], \qquad u_2 \le u; \tag{A11}$$

where "+" in Eq. (A10) is for $r_2 > r_0$ and "-" is for $r_2 \le r_0$.

Case 3: $\beta + (\alpha_j/2) > \pi/2$ (Fig. A5)

$$A_j(u) = 0, \qquad u \le u_0 \tag{A12}$$

$$A_j(u) = 2\pi[1 - (d/cu)], \qquad u_0 < u < u_1 \tag{A13}$$

$$A_j(u) = \pi[1 - \cos(\alpha_j/2)] - \frac{2\theta_1 d}{\sigma u} + 2\cos(\alpha_j/2)\cos^{-1}\left[\frac{\cos\theta_1}{(1-\cos^2\beta\sin^2\theta_1)^{1/2}}\right]$$

$$+ 2\cos^{-1}\left[\cos\beta\csc(\alpha_j/2)\sin\theta_1\right] - 2\cos(\alpha_j/2)\cos^{-1}\left[\frac{\cot(\alpha_j/2)\cos\beta\sin\theta_1}{(1-\cos^2\beta\sin^2\theta_1)^{1/2}}\right],$$

$$u_1 < u < u_2 \qquad \text{(A14)}$$

$$A_j(u) = 2\pi[1 - \cos(\alpha_j/2)], \qquad u \geq u_2; \qquad \text{(A15)}$$

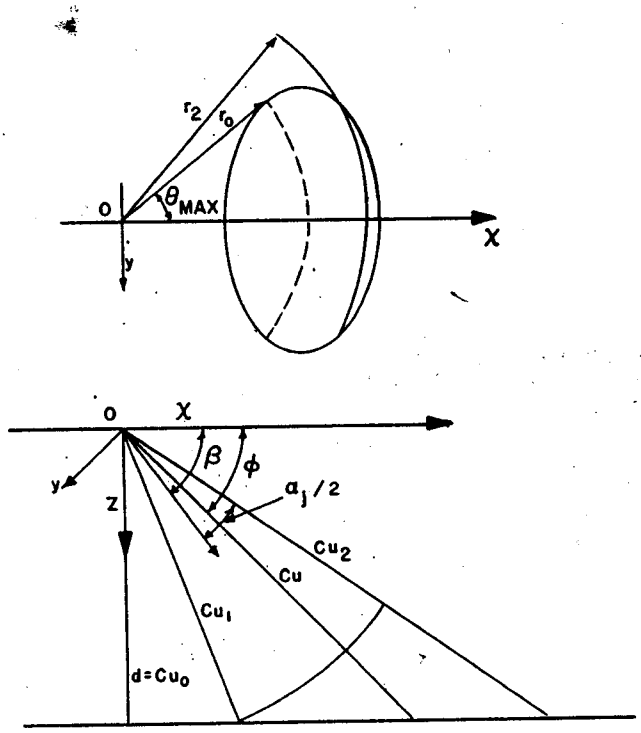

Fig. A4 - Geometry for case 2

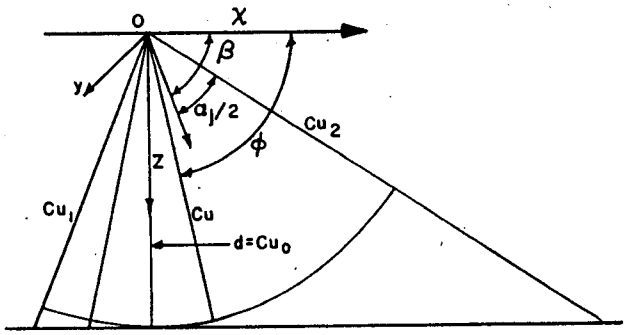

Fig. A5 - Geometry for case 3

where for all three cases

$$u_0 = \frac{d}{c}$$

$$u_1 = \frac{d}{c \sin[\beta + (\alpha_j/2)]}$$

$$u_2 = \frac{d}{c \sin[\beta - (\alpha_j/2)]}$$

$$\cos\theta_1 \cos\beta = \frac{\cos(\alpha_j/2) - \sin\beta \sin\phi}{\cos\phi} = \frac{cu\cos(\alpha_j/2) - d\sin\beta}{(c^2u^2 - d^2)^{1/2}}, \qquad cu > d$$

$$\sin\phi = \frac{d}{cu}$$

$$r_2 = \cos\phi = \frac{(c^2u^2 - d^2)^{1/2}}{cu},$$

and

$$r_0 = [1 - \sec^2(\alpha_j/2)\sin^2\beta]^{1/2}.$$

We now determine $A_j(u)$. Referring to Fig. A1, $r(\theta) = r_1'(\theta) \cup r_1(\theta)$ is a projection of the boundary of a spherical cap on the xy plane. It is then an ellipse of the form

$$\frac{(x-h)^2}{a^2} + \frac{y^2}{b^2} = 1, \qquad a \geq b.$$

It is easy to verify that

$$a = \sin(\alpha_j/2),$$

$$b = \sin(\alpha_j/2)\sin\beta,$$

and

$$h = \cos\beta\cos(\alpha_j/2).$$

Letting $x = r\cos\theta$, $y = r\sin\theta$, we get

$$r(\theta) = \frac{\cos\theta\cos\beta\cos(\alpha_j/2) \pm \sin\beta\left[\sin^2(\alpha_j/2) - \sin^2\theta\cos^2\beta\right]^{1/2}}{1 - \sin^2\theta\cos^2\beta}$$

where "−" $\rightarrow r(\theta) \equiv r_1'(\theta)$ and "+" $\rightarrow r(\theta) \equiv r_1(\theta)$. Also,

$$r_2 = \cos\phi = \frac{(c^2u^2 - d^2)^{1/2}}{cu}$$

$$\cos\theta_1\cos\beta = \frac{\cos(\alpha_j/2) - \sin\beta\sin\phi}{\cos\phi} = \frac{cu\cos(\alpha_j/2) - d\sin\beta}{(c^2u^2 - d^2)^{1/2}}, \qquad cu > d$$

$$r_0 = [1 - \sec^2(\alpha_j/2)\ \sin^2\beta]^{1/2}$$

$$\cos\ \theta_{max} = [1 - \sec^2\beta\ \sin^2(\alpha_j/2)]^{1/2}$$

Then for case 1:

$$\beta = \frac{\pi}{2} \quad \text{and} \quad \cos\ (\alpha_j/2) \le \sin\ \phi$$

or

$$\beta + (\alpha_j/2) > \frac{\pi}{2} \quad \text{and} \quad \cos(\alpha_j/2) \le \sin\ \phi \le -\cos[\beta + (\alpha_j/2)].$$

The area is merely the area of a spherical cap, which is given by

$$A_j(u) = 2\pi[1 - \cos(90 - \phi)] = 2\pi\left(1 - \frac{d}{cu}\right) \tag{A16}$$

or with respect to time t

$$A_j(t) = 2\pi\left(1 - \frac{2d}{ct}\right) \quad \text{and} \quad A_j(t - \tau) = 2\pi\left[1 - \frac{2d}{c(t - \tau)}\right]. \tag{A17}$$

For case 2:

$$\beta + (\alpha_j/2) \le \frac{\pi}{2} \quad \text{and} \quad r_2 \le r_0.$$

Then (see Fig. 2)

$$A_j(u) = 2\int_0^{\theta_1}\int_{r_1'(\theta)}^{r_2} r\sec\gamma\ dr d\theta$$

$$= 2\int_0^{\theta_1} d\theta \int_{r_1'(\theta)}^{r_2} \frac{r\,dr}{\sqrt{1 - r^2}} = -2\int_0^{\theta_1}\left[(1 - r^2)^{1/2}\right]_{r_1'(\theta)}^{r_2} d\theta.$$

Since $r_2 = \cos\ \phi$,

$$A_j(u) = -2\theta_1\sin\phi + 2\int_0^{\theta_1}(1 - [r_1'(\theta)]^2)^{1/2}\ d\theta$$

$$= -2\theta_1\sin\phi + 2\int_0^{\theta_1}\left(1 - \left\{\frac{\cos\theta\cos\beta\cos(\alpha_j/2) - \sin\beta[\sin^2(\alpha_j/2) - \sin^2\theta\cos^2\beta]^{1/2}}{1 - \sin^2\theta\ \cos^2\beta}\right\}^2\right)^{1/2} d\theta$$

$$= -2\theta_1\sin\phi + 2\int_0^{\theta_1}\left\{\frac{\cos\beta\cos\theta[\sin^2(\alpha_j/2) - \sin^2\theta\cos^2\beta)^{1/2} + \cos(\alpha_j/2)\sin\beta}{1 - \sin^2\theta\ \cos^2\beta}\right\} d\theta$$

$$= -2\theta_1\sin\phi + 2\cos(\alpha_j/2)\int_0^{\theta_1}\frac{\sin\beta\,d\theta}{1 - \sin^2\theta\cos^2\beta} + 2\int_0^{\theta_1}\frac{\cos\beta\cos\theta\,[\sin^2(\alpha_j/2) - \sin^2\theta\cos^2\beta]^{1/2}}{1 - \sin^2\theta\cos^2\beta}\,d\theta.$$

The first integral above is of the form #231 in Burington,* and after making the substitution

$$\cos\zeta = \cos\beta\csc(\alpha_j/2)\sin\theta$$

the second integral reduces to form #228. Therefore,

$$A_j(u) = -2\theta_1\sin\phi + 2\cos(\alpha_j/2)\tan^{-1}(\sin\beta\tan\theta_1) + \pi[1-\cos(\alpha_j/2)]$$

$$-2\cos^{-1}[\cos\beta\csc(\alpha_j/2)\sin\theta_1] + 2\cos(\alpha_j/2)\tan^{-1}\left(\frac{\tan\{\cos^{-1}[\cos\beta\csc(\alpha_j/2)\sin\theta_1]\}}{\cos(\alpha_j/2)}\right)$$

or

$$A_j(u) = \pi[1-\cos(\alpha_j/2)] - \frac{2\theta_1 d}{cu} + 2\cos(\alpha_j/2)\cos^{-1}\left[\frac{\cos\theta_1}{(1-\cos^2\beta\sin^2\theta_1)^{1/2}}\right]$$

$$-2\cos^{-1}[\cos\beta\csc(\alpha_j/2)\sin\theta_1] + 2\cos(\alpha_j/2)\cos^{-1}\left[\frac{\cot(\alpha_j/2)\cos\beta\sin\theta_1}{(1-\cos^2\beta\sin^2\theta_1)^{1/2}}\right] \quad \text{(A18)}$$

Equation (A18) can then be converted to $A_j(t)$ and $A_j(t-\tau)$ as in case 1 (i.e., Eq. (A17)) for use in Eq. (A5).

For case 3

$$\beta + (\alpha_j/2) \le \frac{\pi}{2} \quad \text{and} \quad r_2 \ge r_0$$

or

$$\beta + (\alpha_j/2) > \frac{\pi}{2} \quad \text{and} \quad \sin\phi \ge -\cos[\beta + (\alpha_j/2)].$$

Then

$$A_j(u) = 2\pi[1-\cos(\alpha_j/2)] - 2\int_0^{\theta_1}\int_{r_2}^{r_1(\theta)} r\sec\gamma\, dr\, d\theta.$$

As in case 2,

$$A_j(u) = 2\pi[1-\cos(\alpha_j/2)] + 2\int_0^{\theta_1}(1-r^2)^{1/2}\int_{r_2}^{r_1(\theta)} d\theta$$

$$= 2\pi[1-\cos(\alpha_j/2)] - 2\theta_1\sin\phi + 2\int_0^{\theta_1}(1-[r_1(\theta)]^2)^{1/2}\, d\theta$$

$$= 2\pi[1-\cos(\alpha_j/2)] - 2\theta_1\sin\phi +$$

(continued)

*R.S. Burington, "Handbook of Mathematical Tables and Formulas," Sandusky: Handy Publishers, 1948.

$$+ 2\int_0^{\theta_1}\left(1 - \left\{\frac{\cos\theta_1\cos\beta\cos(\alpha_j/2) + \sin\beta[\sin^2(\alpha_j/2) - \sin^2\theta\cos^2\beta]^{1/2}}{1-\sin^2\theta\cos^2\beta}\right\}^2\right)^{1/2} d\theta$$

$$= 2\pi[1 - \cos(\alpha_j/2)] - 2\theta_1\sin\phi$$

$$+ 2\int_0^{\theta_1}\left\{\frac{\cos(\alpha_j/2)\sin\beta - \cos\beta\cos\theta[\sin^2(\alpha_j/2) - \sin^2\theta\cos^2\beta]^{1/2}}{1-\sin^2\theta\cos^2\beta}\right\} d\theta.$$

As in case 2,

$$A_j(u) = \pi[1 - \cos(\alpha_j/2)] - \frac{2\theta_1 d}{cu} + 2\cos(\alpha_j/2)\cos^{-1}\left[\frac{\cos\theta_1}{(1-\cos^2\beta\sin^2\theta_1)^{1/2}}\right]$$

$$+ 2\cos^{-1}[\cos\beta\csc(\alpha_j/2)\sin\theta_1]$$

$$- 2\cos(\alpha_j/2)\cos^{-1}\left[\frac{\cot(\alpha_j/2)\cos\beta\sin\theta_1}{(1-\cos^2\beta\sin^2\theta_1)^{1/2}}\right]. \tag{A19}$$

Finally a conversion similar to cases 1 and 2 of Eq. (A19) to terms of $A_j(t)$ and $A_j(t-\tau)$ is made for use in Eq. (A5).

Appendix B

EFFECTS OF REFRACTION IN DETERMINING SCATTERING STRENGTH

If the medium is isotropic or if the velocity gradient in the medium is sufficiently small, Eq. (9) or Eq. (10) of the text are directly applicable. This is not the case for the medium in which data were taken; therefore the equations were modified to accommodate the refraction. Equation (9) from the text is

$$S = (E - M - G + 20 \log r + Kr + D) - (L + 20 \log i - D - Kr + 10 \log P_i). \tag{B1}$$

Rearranging terms gives

$$S = E - M - G - L - 20 \log i + 2D + 20 \log r + 2Kr - 10 \log P_i. \tag{B2}$$

The last three terms are sensitive to the effects of the anisotropic medium. To take into account the refractive nature of the medium it is convenient to make a series of ray acoustic computations of the propagational factors required. A set of such computations were made for the analysis of the Blake Plateau data. The factors computed (see Fig. B1) were the following:

θ_0 Angle of the ray with respect to the horizontal at the source (degrees)

θ_b Angle of the ray with respect to the horizontal at the bottom (degrees)

d Depth of the bottom below the source (yards)

r_c Distance over the curved path (yards)

x_c Horizontal distance from the source to the point where the ray intersects the bottom (yards)

r_s Distance over the straight path from the source to the bottom (yards)

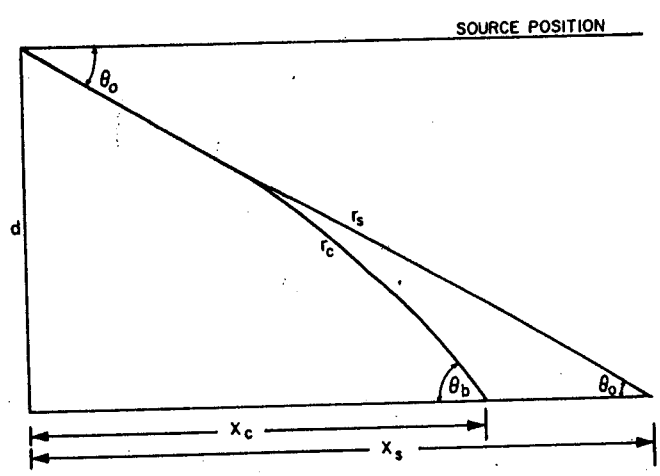

Fig. B1 - Geometry of the propagational factors

x_s Horizontal distance from the source to the bottom for the straight path r_s (yards)

C_v Vertex velocity

t Travel time from the source to the bottom over the r_c path

$\langle C \rangle$ Average sound speed over the r_c path (yards/second)

δd Spreading loss over the r_c path in the downward direction (dB)

δu Spreading loss over the r_c path in the upward direction (dB)

Computation of the above quantities followed Horton's* equations using the conventional method of dividing the sound speed profile into a number of layers of constant gradient or linear sound speed segments. Computations were made with a digital computer, incrementing the depression angle θ through the angles of interest for the depths employed.

It was found that the variation of the average sound speed over the path as a function of angle was less than 1 m/sec for angles between 15 and 90 degrees. This enabled the use of a constant average sound speed of 1666.6 yd/sec for the analysis, having an error of less than 1 part in 3000. Since all measurements were made as a function of time, they were converted to distance using the average sound speed. This applies to Eqs. (A17), (A18), and (A19) in the evaluation of P_i in Appendix A.

In evaluating the spreading loss over the return path, indicated by the term $20 \log r$ of Eq. (B2), it was most convenient to substitute the spreading loss over the upgoing path δu obtained from the computation of propagation factors discussed above. This included both the distance over the curved path and the deviation from inverse square law caused by the refraction.

The straight line distance r in the term $2Kr$ of Eq. (B2) was replaced by the curved path distance r_c from the computations indicated above.

To obtain the average attenuation coefficient K over the path a numerical integration over the depth divided by the depth was made:

$$\langle K \rangle = \frac{1}{d} \int_0^d K(z)\, dz \tag{B3}$$

and

$$K = 10 \log \langle K \rangle \tag{B4}$$

where $K(z)$ is the function relating absorption and depth. The effects of pressure and change of salinity with depth were considered. The absorption versus depth was obtained by combining the temperature versus depth curve (also employed in the propagation computations) and the salinity profiles, using DelGrosso's† tabulation of absorption for various values of temperature and salinity. The Schulkin and Marsh‡ equation was used in taking account of pressure. The value of $\langle K \rangle$ used in the analysis was 2.268×10^{-3} dB/yd.

*J.W. Horton, "Fundamentals of Sonar," U.S. Naval Institute, NavShips 92719, 1957.
†V.A. DelGrosso, "Dependence of Sound Absorption on Concentration, Frequency, and Temperature in $MgSo_4$ Solutions Equivalent to Sea Water - Graphs from Calculations Based on a Review," NRL Report 4279, Jan. 1954.
‡M. Schulkin and H.W. Marsh, "Sound Absorption in Sea Water," J. Acoust. Soc. Am. 34: 864 (1962).

Pertinent constants of the system and the environment used in the analysis were the following: (a) the fixed gain in the receiving system was G = 30.6 dB, (b) the dome loss was D = 1 dB, (c) the water depth was d = 880 yd, (d) the transducer characteristics, which are pressure and temperature sensitive, were as given in Table B1 at the temperature and depth used, and (e) the source levels for the experiment were in the range of 117.6 to 121.0 dB.

Table B1
Transducer Characteristics

Transducer Depth (yd)	Receiving Sensitivity M (dB//μbar/v)	Transmitting Response L (dB//μbar/amp at 1 yd)
18	-74.2	106.4
33	-75	105.6

The conversion from depression angle β to grazing angle δ at the bottom is obtained from the computation of the propagation factors, making the scattering strength measurements independent of the medium refraction.

Appendix C

SERVICES

Commander, Operational Test and Evaluation Force, has provided the following aid in the acquisition of data for the experimental portion of this report. The operations were conducted under Project D/S-34, during the period August 28, 1961, through September 14, 1961.

USS Grouper (AGSS-214) was available 18 days operating and in transit plus 10 days at the pier for installation and removal of instrumentation.

Security Classification

DOCUMENT CONTROL DATA - R & D

(Security classification of title, body of abstract and indexing annotation must be entered when the overall report is classified)

1. ORIGINATING ACTIVITY (Corporate author)

Naval Research Laboratory
Washington, D.C. 20390

2a. REPORT SECURITY CLASSIFICATION

Unclassified

2b. GROUP

3. REPORT TITLE

EFFECT OF GEOMETRY ON ACOUSTIC MONOSTATIC SCATTERING FROM THE OCEAN BOTTOM

4. DESCRIPTIVE NOTES (Type of report and inclusive dates)

An interim report on a continuing problem.

5. AUTHOR(S) (First name, middle initial, last name)

Burton G. Hurdle and Kenneth D. Flowers

6. REPORT DATE

March 16, 1967

7a. TOTAL NO. OF PAGES

30

7b. NO. OF REFS

10

8a. CONTRACT OR GRANT NO.

NRL Problem S01-12

b. PROJECT NO.

RF 101-03-44-4059

c.

SF 101-03-15-8181

d.

9a. ORIGINATOR'S REPORT NUMBER(S)

NRL Report 6517

9b. OTHER REPORT NO(S) (Any other numbers that may be assigned this report)

10. DISTRIBUTION STATEMENT

Distribution of this document is unlimited.

11. SUPPLEMENTARY NOTES

12. SPONSORING MILITARY ACTIVITY

Department of the Navy (Office of Naval Research and Naval Ship Systems Command), Washington, D.C. 20360

13. ABSTRACT

An investigation was made to determine the degree of correspondence between measured returns scattered from the ocean bottom and an extended model of isotropic scattering from a boundary. The isotropic scattering model was applied to yield the form of the scattered intensity as a function of time for the monostatic geometry in which a circular symmetric beam function is employed. An experiment was conducted in the Blake Plateau area with a piston transducer operated at 19.5 kHz and having a beamwidth of approximately 8 degrees at the half-power points. Measured signal intensities from the relatively flat bottom in this area were averaged and compared with those of the model. These comparisons were made for depression angles between 15 and 90 degrees, and for pulse lengths between 2 and 3000 msec. Measured and computed curves were found to be essentially congruent for the range of pulse lengths and depression angles employed. However, for a given depression angle it is found that scattering strength, the acoustic constant used to characterize the boundary, varies with pulse length. This indicates that scattering from the Blake Plateau bottom is not isotropic. Measurements of scattering strength versus grazing angle for the Blake Plateau area were obtained.

DD FORM 1 NOV 65 1473 (PAGE 1)

S/N 0101-807-6801

Security Classification

14. KEY WORDS	LINK A ROLE	LINK A WT	LINK B ROLE	LINK B WT	LINK C ROLE	LINK C WT
Underwater sound						
Sound transmission						
Ocean bottom						
Scattering						
Underwater sound signals						
Monostatic geometry						
Theory						
Experimental data						
Scattering strength						
Pulse length						
Depression angle						